Screening of false induction motor fault alarms produced by axial air ducts based on the space-harmonic-induced current components

Screening of False Induction Motor Fault Alarms Produced by Axial Air Ducts based on the Space Harmonic-Induced Current Components

Chanseung Yang, *Student Member, IEEE,* Tae-June Kang, *Student Member, IEEE,*
Sang Bin Lee, *Senior Member, IEEE,* and Ji-Yoon Yoo
Alberto Bellini, *Member*, *IEEE*, Luca Zarri, *Senior Member*, *IEEE*, Fiorenzo Filippetti, *Member*, *IEEE*

***Abstract*—Motor Current Signature Analysis based on the 50/60 Hz sidebands has become a common test in industry for monitoring the condition of the induction motor rotor cage. However, many cases of unnecessary motor inspection or outage due to false alarms produced by rotor axial duct interference have been reported. If the number of *axial ducts* and *poles* are identical, this can produce 50/60 Hz sideband frequency components in Motor Current Signature Analysis that overlap with that of rotor faults, resulting in false alarms. However, there currently is no practical test method available for distinguishing rotor faults and false indications other than testing the rotor off-line or under the startup transient. In this paper, the feasibility of using the rotor fault frequency component produced by the space harmonic waves is evaluated as a solution for the first time. Since the 5th or 7th space harmonics have a spatial distribution of flux that do not penetrate in the rotor yoke to reach the axial ducts, they do not produce false alarms. The proposed method is verified on 6.6 kV motors misdiagnosed with broken bars via the 50/60 Hz sidebands of Motor Current Signature Analysis. It is shown that it provides reliable on-line indication of rotor faults independent of axial duct influence, and can be used for screening out false alarms.**

***Index Terms*—Condition Monitoring, Fault Diagnosis, Frequency Domain Analysis, Induction Motor, Predictive Maintenance.**

NOMENCLATURE

N_p, N_d	Number of poles and rotor axial air ducts.
N_s, N_r	Number of stator and rotor slots.
f_s	Supply electrical frequency in hertz.
h	h^{th} space harmonic order.
s	Rotor slip.
f_{duct}, $f_{brb,h}$	MCSA frequency sidebands produced by axial duct and broken bar due to h^{th} space harmonic in hertz.
k, m	Positive integers.
i_s, i_m, i_r	Stator, magnetizing, and rotor currents.
ϕ_e	Electrical angle of broken bar location measured with respect to the axial duct in the direction of rotor rotation.
f_h, $f_{h,r}$	Frequency (speed) of h^{th} order space harmonic wave with respect to stator and rotor in hertz.
$k_{p,h}$	Stator pitch factor for h^{th} space harmonic component.

Manuscript received January 27, 2014; revised April 11, 2014 and May 13, 2014; accepted May 20, 2014.

Sang Bin Lee, Chanseung Yang, Tae-June Kang, and Ji-Yoon Yoo are with Korea University, Seoul, Korea (e-mail: sangbinlee@korea.ac.kr; y1c2s@korea.ac.kr; magnuskt@korea.ac.kr; jyyoo@korea.ac.kr).

Alberto Bellini, Luca Zarri, and Fiorenzo Filippetti are with University of Bologna, Bologna, Italy (e-mail: a.bellini@unibo.it; luca.zarri2@unibo.it; fiorenzo.filippetti@unibo.it).

I. INTRODUCTION

MOTOR current signature analysis (MCSA) is one of the most popular tools for monitoring the condition of the rotor cage of medium/high voltage (MV/HV) induction motors. The on-line and remote monitoring capability of MCSA makes it an attractive and convenient technology in an industrial environment [1]-[6]. However, false rotor fault alarms for healthy motors can be caused by rotor axial ducts, rotor ovality, low frequency load oscillations, or porosity (aluminum die cast rotors) when the 50/60 Hz sidebands are used, as reported in [4]-[11]. A false alarm can result in an unnecessary and costly inspection or outage of the motor and driven process. The cost of inspection for MV/ HV motors with a false alarm is typically tens of thousands of dollars excluding the cost of repair and loss of production (if stand-by or spare motors are available) [9]-[11].

One of the most common root causes of false rotor fault alarms is the interference caused by rotor axial air ducts. Rotor air ducts, shown in Fig. 1, are employed in motors rated above 100 kW for effective cooling of the rotor, and reduction in inertia and material costs [9]-[10]. Axial ducts can cause the magnetic reluctance of the flux path to be asymmetric since the flux can penetrate inside of the axial ducts depending on the relative position between the flux and rotor, as illustrated in Fig.1. The difference in the flux path can be seen in the results

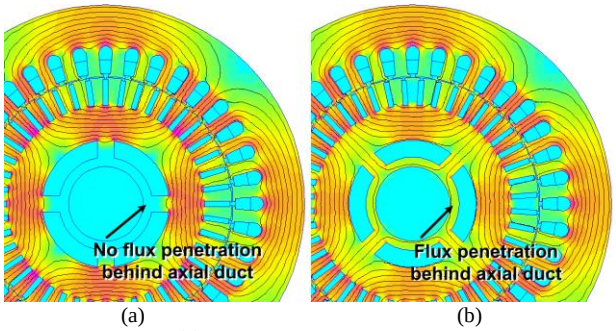

Fig. 1 FE analysis of flux distribution in 4 pole motor with 4 axial air ducts (N_d=N_p=4) when magnetic poles and duct arms are electrically (a) 90° apart and (b) aligned (0°) under steady state operation. The asymmetry in magnetic flux path produces false rotor fault alarm.

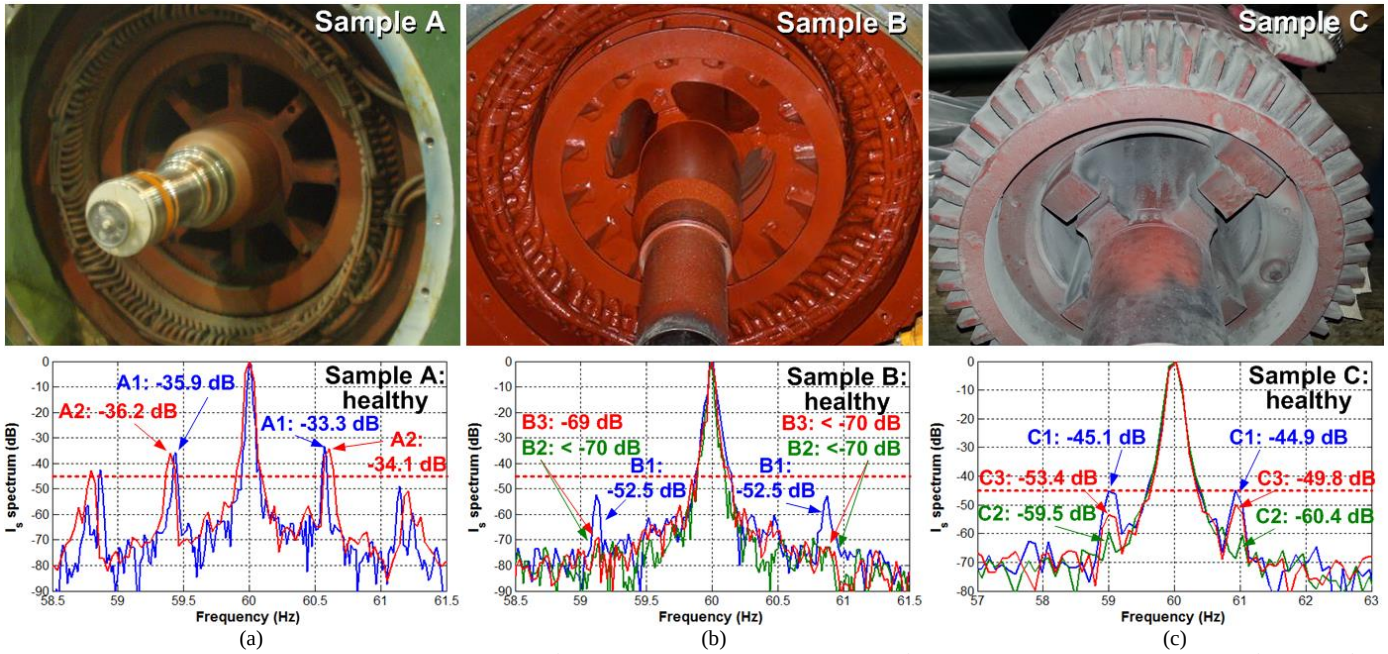

(a) (b) (c)

Fig. 2. Rotor (upper) and stator current, I_s, spectrum (lower) of 6.6 kV motors with identical number of *rotor air ducts*, N_d, and *poles*, N_p with false rotor fault alarms produced with MCSA; (a) Sample A (A1, A2): 2400 kW, 8 pole induced draft fan motor (N_d=N_p=8); (b) Sample B (B1, B2, B3): 280 kW, 4 pole, condensate pump motor (N_d=N_p=4); (c) Sample C (C1, C2, C3): 350 kW, 4 pole condensate pump motor (N_d=N_p=4)

of the 2 dimensional finite element (FE) analysis in Fig. 1(a)-(b) for a 4 pole motor with 4 axial ducts (high reluctance path in Fig. 1(a) and low reluctance path in Fig. 1(b)). The variation in the magnetic reluctance results in modulation of the magnetizing current, i_m, whereas variation in rotor resistance due to broken bars produce modulation in the rotor current, i_r. Modulation of i_m can produce components at f_{duct} in the current spectrum that are identical to the rotor fault frequency, $f_{brb,1}$, if the number of air ducts, N_d, and poles, N_p, are the equal as,

$$f_{duct} = f_{brb,1} = (1 \pm 2ks) f_s \,, \tag{1}$$

where f_s is the supply frequency, s is the rotor slip, and k is a positive integer. This can be misinterpreted as broken rotor bars when the 50/60 Hz sideband-based MCSA (hereinafter referred to as MCSA) is applied, as reported in [5]-[11].

Three recent cases of false MCSA rotor fault alarms produced by the axial duct influence are shown in Fig. 2 for 6.6 kV induction motors [9]-[11]. The results of MCSA performed on the three motor samples (samples A, B, and C) indicated broken bars in some of the rotor samples. However, inspection of the rotors showed that the bars are in healthy condition for all motor samples. This resulted in unnecessary expenditures for the inspection, where the cost of inspection alone exceeded 100,000 dollars for the 2.4 MW motor of Fig. 1(a). False MCSA alarms due to axial ducts is a common on-going problem in the field, considering that a large portion of MV/HV motors are of N_d=N_p design, according to the investigation in [9]. In most cases, it is unknown whether a motor is of N_d=N_p design unless the motor is disassembled. If a motor is of N_d=N_p design, it does not necessarily produce the $f_{brb,1}$ component since this depends on the rotor design and construction, material characteristics, and operating conditions [9].

A number of researchers have worked on separating the influence of the rotor fault and air duct in [5]-[10] for screening out false alarms to prevent unnecessary and costly motor inspection. In [5]-[7], it is suggested that the $f_{brb,1}$ component be compared under two different load conditions. Since it is the modulation of the magnetizing current that produces the false indication, the $f_{brb,1}$ components decrease with increase in load, if produced by axial ducts. Although this could screen out false alarms for healthy motors, it cannot provide reliable assessment for faulty motors, as will be shown in II. In [8], a method for separating the two effects on-line based on a mathematical model was proposed. However, the requirement of data under multiple load conditions is not feasible for many industrial applications, and is a limitation of the methods presented in [5]-[8]. In [9]-[11], it is shown that broken bars can be detected reliably independent of axial ducts if tested under high slip (off-line standstill [9], startup transient [10]) conditions since there is no flux penetration in the rotor (cage eddy current rejection), as shown in Fig. 3(a). The limitation of off-line tests is the requirement of motor disassembly or manual shaft rotation for testing, which makes frequent, automated, and remote motor testing difficult [12]. It is also difficult to perform a startup test for applications that are run continuously.

It is clearly shown in the analysis presented in [9] and the arguments above that a false alarm due to axial ducts is common and the consequence can be serious. It is also shown in [9]-[11] that there currently is no practical method available for screening out false alarms when the motor is operating. Based on the fact that the space harmonic flux cannot penetrate into the air ducts to produce asymmetry, the objective of this paper is to investigate the feasibility of using the space harmonics-induced rotor fault components. An experimental study on custom built 380 V and 6.6 kV motors with false alarms show that the proposed method provides reliable

detection of rotor faults independent of the axial duct influence.

II. Influence of Rotor Axial Air Ducts on MCSA

A. False Rotor Fault Alarms – Case Studies

The MCSA results of the stator current, I_s, spectrum for the healthy 6.6 kV motors (N_d=N_p) with false broken bar alarms are shown in Fig. 2. The three 6.6 kV motors in Fig. 2(a)-(c), denoted as samples A, B, and C, are fan or pump motors operating in power generation plants. For the critical HV motors in power plants, multiple motors are operated in parallel to share the load, and stand-by motors of identical design are often installed to minimize the impact of motor failure. MCSA measurements for samples A, B, and C were obtained from all the identical motor units available. The ratings, application, and the figure where test results are shown, are summarized in Table I. For the 2400 kW induced draft fan motor, both samples A1 and A2 showed strong $f_{brb,1}$ sidebands between -37 and -33 dB, respectively, in the current spectrum (Fig. 2(a)). This exceeds the -45 dB fault threshold level commonly used in the field. Vibration analysis also indicated rotor faults; however, motor inspection did not reveal any signs of rotor bar or end ring damage.

For the 280 kW and 350 kW condensate pump motor samples B and C, the MCSA measurements of the $f_{brb,1}$ components for three identical units were not consistent, as can be seen in Fig. 2(b)-(c). The $f_{brb,1}$ components were -52.5 dB for sample B1, and below -69 dB for samples B2 and B3. For samples C1, C2, and C3, the $f_{brb,1}$ components were spread out between -45 dB and -60 dB, as shown in Fig. 2(c). Rotor faults were strongly suspected for samples B1 and C1 considering that the $f_{brb,1}$ components were significantly higher than that of the motors of identical design. Since the sample B1~B3 and C1~C3 motors were manufactured and commissioned at the same time and operated under similar load, it was natural to conclude that it is very unlikely for the motors to have larger $f_{brb,1}$ components unless a rotor fault is present. However, the results of off-line inspection and testing showed that both rotors for samples B1 and C1 were in good condition.

The single phase rotation test was performed on samples B1, B2, and C1 with 380 V applied between two terminals for pulsating field excitation [12]. The results of the current measurements as a function of the rotor position shown in Fig. 3(b) imply that there is no asymmetry in the rotor cage. If a broken bar is present, the current fluctuates N_p times, as the rotor is rotated one revolution due to the variation in the rotor impedance. The reason why the single phase test is not influenced by the axial ducts is the limited flux penetration into the rotor yoke under standstill conditions, as shown in Fig. 3(a). The inconsistency in the $f_{brb,1}$ components for samples B and C is suspected to be caused by part-to-part variation introduced due to component- or manufacturing- tolerances such as the variance in the Si-Fe lamination magnetic characteristics [9]. It was concluded based on the inspection and test results that the false positive indication for samples A, B, and C was due to the axial air ducts for the N_d=N_p motors.

B. Screening of False Alarms due to Axial Air Duct Influence

It is difficult to screen out false MCSA rotor fault alarms because the axial ducts and broken bars produce the same frequency component in the stator current when performing MCSA. The two components interact, since the $f_{brb,1}$ components measured in the stator current, $i_{s,brb,1}$, is the sum of the two current components shown in (2).

$$i_{s,brb,1} = i_{m,brb,1} + i_{r,brb,1} \tag{2}$$

The $f_{brb,1}$ components produced by the axial ducts, $i_{m,brb,1}$, and by the broken bars, $i_{r,brb,1}$, have a different phase angle depending on the location of the fault with respect to the axial duct. The electrical angle measured with respect to the center of the axial duct in the direction of rotor rotation is denoted as ϕ_e, is shown in Fig. 3(a). It was shown in [9] that the magnitude of $i_{s,brb,1}$ is a function of the magnitudes of $i_{m,brb,1}$, $i_{r,brb,1}$, rotor slip, and angle ϕ_e, as shown in (3).

$$I_{s,brb,1} = \sqrt{I_{m,brb,1}^2 + 2I_{m,brb,1}I_{r,brb,1}s\sin(2\phi_e) + I_{r,brb,1}^2 s^2} \tag{3}$$

A simulation was performed to illustrate how the values of $I_{s,brb,1}$ varies with fault location ϕ_e, as shown in Fig. 4. The values of $I_{s,brb,1}$ as a function of slip were calculated from (3) for a number of different values of ϕ_e. In Fig. 4, it was assumed that $I_{m,brb,1} = 2I_{r,brb,1}$ based on the ratio observed for samples D and E (shown in IV) when 1 of 44 bars are broken. It can be clearly seen in Fig. 4 and (3) that $f_{brb,1}$ components in the stator current are influenced significantly by the location of the rotor fault, ϕ_e, in addition to the slip (load) and magnitudes of $i_{m,brb,1}$ and $i_{r,brb,1}$. The $I_{s,brb,1}$ component shows maximum increase, if

Table I. Ratings, application, and test results for field and lab motor samples

Sample	P (kW)	V (V)	N_d / N_p	Application	Rotor Photo (Fig.)	MCSA $f_{brb,1}$ (Fig.)	MCSA $f_{brb,5}$ (Fig.)
A (A1~A2)	2400	6600	8	Induced draft fan	2(a)	2(a)	-
B (B1~B3)	280	6600	4	Condensate pump	2(b)	2(b), 15	15(a)
C (C1~C3)	350	6600	4	Condensate pump	2(c)	2(c), 15	15(b)
D	5.5	380	4	Laboratory	7(a)	8	9, 10
E	5.5	380	4	Laboratory	7(b)-(c)	11	12-13
F(F1,F2)	5.5	380	0/4	Laboratory	-	14	14

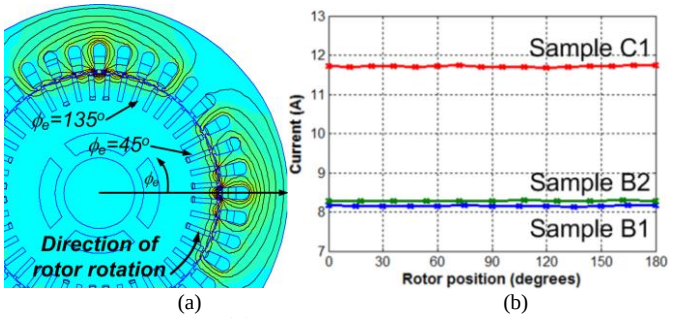

(a) (b)

Fig. 3. (a) FE analysis of flux distribution under 60 Hz excitation at motor standstill; (b) single phase rotation test results (current vs. rotor position) on sample B1, B2, and C1 under 380 V pulsating field excitation at motor standstill

the bar is broken at the ϕ_e=45° location, whereas it shows maximum decrease when ϕ_e=135°, as shown in Fig. 4. This is observed because the $i_{m,brb,1}$ and $i_{r,brb,1}$ components are in phase (add) when ϕ_e=45°, and out of phase (cancel) when ϕ_e=135° [9]. If the fault is located at ϕ_e=135°, $I_{s,brb,1}$ initially decreases, but starts to increase if the magnitude of the $i_{r,brb,1}$ component exceeds that of $i_{m,brb,1}$. As a result, the $f_{brb,1}$ component measured in the current can be anywhere in the highlighted region of Fig. 4 depending on the slip (load) and ϕ_e for a given $I_{m,brb,1}$ and $I_{r,brb,1}$. Therefore, the $f_{brb,1}$ component can increase, decrease, or remain unchanged, if a broken bar is present in a N_p=N_d motor with axial duct influence.

If a rotor fault alarm is given by MCSA, one must check if it is caused by a broken bar or axial ducts (false alarm). The easiest solution is to check N_d, if possible, to rule out the axial duct induced false alarm. Otherwise, the best option is to run an off-line or startup test, but there are many limitations to performing these tests. The remaining options are to observe the trend of how the MCSA measurements change with load, time, or other motors of identical design. However, Fig. 4 and (3) clearly show that comparing the $i_{s,brb,1}$ magnitudes at two different loads suggested in [5]-[7] is invalid, since $I_{s,brb,1}$ can decrease with increase in load, if the bar is broken in the vicinity of ϕ_e=135°. Trending the values of $I_{s,brb,1}$ over time to observe an increase for broken bar indications is also invalid since $I_{s,brb,1}$ can decrease with a broken near ϕ_e=135°. It can be seen from the MCSA results of samples B1~B3, and C1~C3 of Fig. 2(b)-(c) that comparison between motors of identical design cannot be used for screening out false alarms. The false rotor fault indication in samples B1, C1 is not present for samples B2, B3, and C2 due to the variance in the characteristics of individual motors [9]. The case studies and analysis presented in this section clearly shows that the $f_{brb,1}$ component does not provide sufficient information necessary for screening out false alarms due to axial ducts.

III. Reliable Detection of Rotor Faults Based on the 5TH Order Space Harmonics-based MCSA Components

It is clear from the arguments in II that MCSA cannot provide reliable detection of broken bars for $N_p = N_d$ motors. For such motors, rotor faults can only be detected reliably with off-line standstill or startup transient tests, where the motor is excited under high slip conditions [9]-[10]. With high slip excitation, flux penetration in the rotor is limited due to cage eddy current rejection as shown in Fig. 3(a); therefore, the flux cannot reach the axial ducts. However, these tests cannot be performed on-line when the motor is running. Considering that the slip between the rotor and space harmonic flux is high, monitoring of the space harmonics induced rotor fault components is considered in this paper under the expectation that it is immune to false alarms due to axial ducts.

A. Rotor Fault Components Induced by Space Harmonics

It is shown in a number of resources that stator winding space harmonic waves produce rotor fault components, $f_{brb,h}$, shown in (4) in the stator current spectrum when performing MCSA. The $f_{brb,h}$ sidebands can be observed for k_2 = 5,7,11,13,…, if broken bars are present [4].

$$f_{brb,h} = (k_2(1-s) \pm s) f_s \tag{4}$$

The non-ideal (*i.e.* non-sinusoidal) distribution of the stator winding produces the fundamental component and a series of odd space harmonic, h, magneto-motive forces (MMF) in the machine, even for an ideal balanced 3 phase sinusoidal input. The MMF contains space harmonics of order h=6m±1 (m=1,2,…), where MMFs rotate in the same (positive) direction as the fundamental wave for h=6m+1 (h= 7,13,…), and in the opposite (negative) direction for h=6m-1 (h= 5,11,…) as,

$$h = \begin{cases} 6m+1 \ \ (\textit{positive direction}, h = 7,13,\ldots) \\ 6m-1 \ \ (\textit{negative direction}, h = 5,11,\ldots) \end{cases} (m = 1,2,\ldots). \tag{5}$$

The h^{th} space harmonic MMF wave is equivalent to a machine with $h \cdot N_p$ poles considering the spatial distribution of flux. This can be seen in the FE analysis of the 5th order harmonic flux distribution in a 4 pole motor generated by splitting up the stator winding into that of a 20 pole stator in Fig. 5. The h^{th} space harmonic wave rotates at a speed (frequency), f_h, of 1/h of the fundamental wave as, shown in (6) [13], where the sign of h-6m represents the direction of rotation.

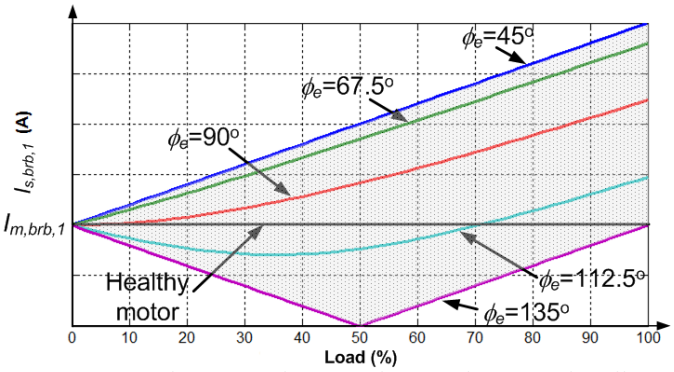

Fig. 4. Example of the values of $I_{s,brb,1}$ as a function of slip (load) for different ϕ_e calculated from (3) for faulty rotor (assuming $I_{m,brb,1} = 2I_{r,brb,1}$)

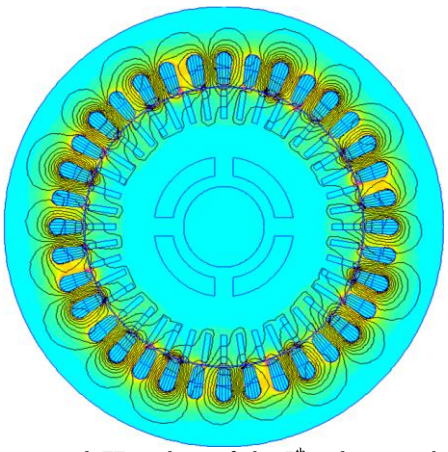

Fig. 5. 2 dimensional FE analysis of the 5th order space harmonic flux distribution for 4 pole motor under rated slip operation

$$f_h = (h-6m) f_s / h . \quad (6)$$

The speed (frequency) of the space harmonic waves with respect to the rotor, $f_{h,r}$, can be expressed as the difference between the speed of the h^{th} space harmonic wave and rotor as

$$f_{h,r} = f_h - (1-s) f_s . \quad (7)$$

It can be seen from (7) that the speed of the fundamental, 5th, and 7th order space harmonic waves with respect to the rotor are sf_s, $-6/5f_s+sf_s$, and $-6/7f_s+sf_s$, respectively. This shows that the difference in the speed of the 5th and 7th space harmonic waves and the rotor is large compared to that of the fundamental wave. This results in high slip excitation of the rotor with $h \geq 5$, and makes penetration of the space harmonic flux into the rotor yoke difficult due to eddy current rejection of the rotor cage. It can be observed in the FE analysis of Fig. 5 that the 5th order harmonic flux simulated to rotate at $-6/5f_s+sf_s$ does not reach the axial ducts, and therefore, does not produce false alarms as in the case of the fundamental wave shown in Fig. 1. This is similar to the reliable test methods such as the single phase rotation test or startup transient test where the fundamental flux does not penetrate into the rotor yoke, as shown in Fig. 3(a). The space harmonics sideband based MCSA has a significant advantage over existing methods in that it can provide reliable monitoring of the fault when the motor is operating.

If a fault is present in the rotor cage, the rotating fundamental and space harmonic fields create anomalies in the magnetic field that produce a pulsating field with respect to the rotor at frequencies of $f_{h,r}$ [4]. The pulsating field can be decomposed into two rotating fields in opposite direction ($\pm f_{h,r}$) according to the double revolving field theory. The h^{th} space harmonic fields created by the fault induce $f_{brb,h}$ frequency components in the stator winding in a manner similar to the fundamental wave as

$$f_{brb,h} = (1-s) f_s \pm f_{h,r} \cdot h = \begin{cases} (1-6m) \cdot f_s + (h-1) \cdot sf_s , \\ (1+6m) \cdot f_s - (h+1) \cdot sf_s \end{cases} \quad (8)$$

where the equation is derived from (5)-(7). The principle behind the induction of the $f_{brb,h}$ components in the stator current derived in (5)-(8) is illustrated in Fig. 6 for the fundamental and 5th, 7th space harmonics. The frequency of the h^{th} space harmonic wave with respect to the stator and rotor, f_h and $f_{h,r}$, and the sideband components induced in the stator winding as a result of broken bars, $f_{brb,h}$, are summarized in Table II for the fundamental and 5th, 7th, 11th, and 13th space harmonics. The direction of rotor rotation is considered 'positive' in the $f_{brb,h}$ components in Table II. It can be seen in Fig. 6 and Table II that the induction of the $f_{brb,h}$ components due to the space harmonics are the same, in principle, as that of the fundamental component. The $f_{brb,h}$ sidebands derived in (8) are identical to the components shown in (4), if MCSA is performed using one phase of the current, where the direction of rotation cannot be discerned. The flux distribution shown in Fig 5 clearly shows that the $f_{brb,h}$ components can provide reliable detection of rotor faults, and the derivation of the $f_{brb,h}$ components are shown in Fig. 6 and Table II to support the analysis.

B. Expected Advantages and Limitations of Proposed Method

The main advantage expected from monitoring the space harmonics related rotor fault components with MCSA is its immunity to the false alarms produced by axial ducts. The space harmonics induced $f_{brb,h}$ component can be monitored on-line during motor operation to screen out false alarms produced by the $f_{brb,1}$ sidebands commonly used. This provides a significant advantage over test methods that require the motor to be stopped for standstill testing or to be started to observe the transient. Monitoring of the space or time harmonics induced sidebands have been studied in [14]-[19] for different purposes. In [14]-[15], the potential of using the $f_{brb,h}$ components for reliable detection of non-adjacent broken bars is evaluated. It is shown that non-adjacent broken bars separated 90 electrical degrees apart unobservable with the $f_{brb,1}$ component could be observed with $f_{brb,h}$, since the pattern of broken bars that are symmetrical to the fundamental flux is asymmetric to the space harmonic flux pattern. It is also shown that space [16]-[18] or time [19] harmonics based detection of rotor faults is insensitive to load variations, inertia, or supply distortion or unbalance, and not influenced by load oscillations. The feasibility of using this component for reliable fault detection independent of the influence of axial ducts is studied in this paper for the first time. The advantages of using the $f_{brb,h}$ component studied in [14]-[18] listed above apply to the proposed method.

A potential shortcoming of monitoring the $f_{brb,h}$ component is the difficulty of determining the fault threshold. The fault threshold for the $f_{brb,1}$ component has been studied extensively

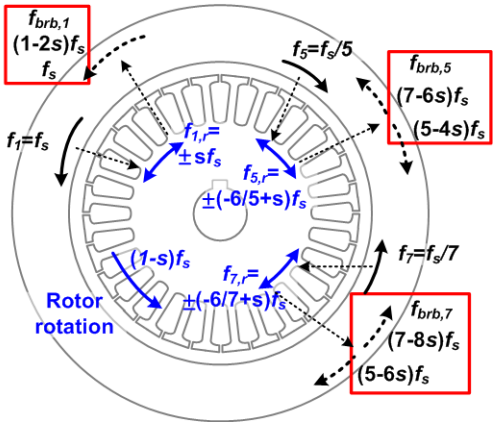

Fig. 6. Principle behind induction of $f_{brb,h}$ components in the stator current for the fundamental and 5th, 7th space harmonics

Table II. Summary of f_h, $f_{h,r}$, and $f_{brb,h}$ for fundamental, 5th, 7th, 11th, and 13th space harmonics (+ represents direction of rotor rotation)

h	f_h	$f_{h,r}$	$f_{brb,h}$
	$(h-6m)f_s/h$	$f_h-(1-s)f_s$	$(1-s)f_s \pm f_{h,r}h$
1	f_s	sf_s	$(1-2s)f_s$, f_s
5	$-f_s/5$	$(-6/5+s)f_s$	$-(5-4s)f_s$, $(7-6s)f_s$
7	$f_s/7$	$(-6/7+s)f_s$	$-(5-6s)f_s$, $(7-8s)f_s$
11	$-f_s/11$	$(-12/11+s)f_s$	$-(11-10s)f_s$, $(13-12s)f_s$
13	$f_s/13$	$(-12/13+s)f_s$	$-(11-12s)f_s$, $(13-14s)f_s$

in academia and determined based on experience accumulated in the field with MCSA technology over the years [4], [6], [20]-[23]. The $f_{brb,h}$ components will increase with fault severity; however, the degree of increase is expected to depend heavily on the magnitude of the specific space harmonic component in the stator winding. This depends on the winding design factors such as the pitch factor and distribution factor, which are unknown to the field maintenance engineer. Therefore, a reliable way of monitoring the rotor condition is to trend the increase in multiple $f_{brb,h}$ components over time, and observe it in conjunction with the $f_{brb,1}$ component.

IV. Experimental Results

A. Experimental Setup

An experimental study was performed to verify the validity of space harmonics based MCSA for reliable monitoring of rotor faults independent of the axial duct influence. The proposed method was verified for the 6.6 kV field samples B and C, and on custom built lab samples D, E, and F. Two 380 V, 5.5 kW motors with N_d=N_p rotor samples (D and E) were custom-built to verify the effectiveness of the method under controlled fault conditions in the lab. The axial ducts of sample D were created by drilling 20 holes in the yoke to produce 4 groups of axial ducts in the yoke of an *Al* die-cast rotor, as shown in Fig 7(a). A fabricated *Cu* bar rotor with N_d=4 shown in Fig. 7(b) was designed and built from the laser cut laminations of Fig. 7(c) to fit the stator of sample D, as it is representative of HV motors.

The stator of samples D, E, and F1 have 36 stator slots with 7/9 fractional pitch. To observe how the space harmonic content of the stator winding influences the increase in $f_{brb,h}$, one of the 380 V, 5.5 kW stators identical to samples D, E, and F1 was rewound with a full pitch winding (sample F2) with the same number of turns. The stator structure and pitch factor for the fundamental, 5th, and 7th space harmonics for samples D, E, and F are summarized in Table III.

For samples D, E, and F, up to 3 of 44 contiguous *Al* or *Cu* bars were cut at the bar and end ring joint to simulate broken bars. To test under the condition where the $i_{m,brb,1}$ and $i_{r,brb,1}$ components are in phase (add), bars at the ϕ_e=45° location shown in Fig. 4(b) were cut. The case where the $i_{m,brb,1}$ and $i_{r,brb,1}$ components are out of phase (cancel, ϕ_e=135°) was also tested by rotating the same rotor used for the ϕ_e=45° case in the opposite direction. This is equivalent to the broken bar being located at ϕ_e=135°. The test results for the healthy rotor are different in Figs. 8, 10, 11, 13 for the cases of ϕ_e=45° and ϕ_e=135° for this reason. It was not possible to damage the rotor bars of samples B or C since they are HV motors operating in the field. The information regarding the rotors and test results for motor samples A~F is summarized in Table I. The load of motor was controlled by adjusting the field voltage of a 22.5 kW DC generator coupled to the motor. Commercial current sensors and a data acquisition board were used to measure the current at 6 kHz sampling for 60 *s* under steady state conditions with MCSA.

B. Experimental Results

MCSA testing was performed with the motor operating under 10~100% rated load with 0~2 broken bars located at ϕ_e=45° and 135° for samples D and E (healthy rotor refers to the rotor with 0 broken bars). The interaction between the broken bar and axial duct influence can be seen in the measurements of the (1-2*s*) f_s components of sample D in Fig. 8. It can be observed that $I_{s,brb,1}$ increases if the bar is broken at the ϕ_e=45° location (Fig 3(a)) because the $i_{m,brb,1}$ and $i_{r,brb,1}$ components are in phase (add). $I_{s,1-2s}$ decreases (and then increases) if ϕ_e=135° because $i_{m,brb,1}$ and $i_{r,brb,1}$ are out of phase (cancel). The pattern of $I_{s,brb,1}$ in Fig. 8 is consistent with the simulated results shown

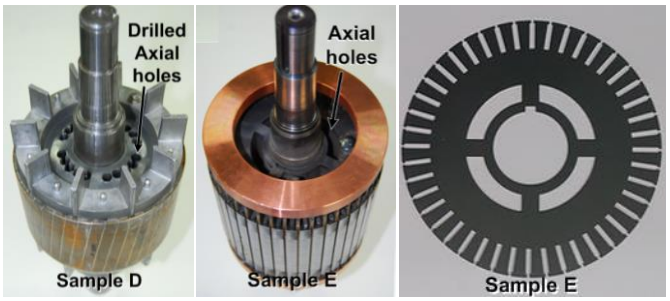

(a) (b) (c)

Fig. 7 (a) *Al* die-cast rotor with 4 drilled axial holes (sample D); (b) fabricated *Cu* rotor with 4 laser cut axial holes (sample E); (c) rotor lamination for sample E

Table III. Stator winding structure and pitch factor for fundamental, 5th, and 7th space harmonics for samples D, E, and F

Sample	N_s	N_r	Coil pitch	$\|k_{p,1}\|$	$\|k_{p,5}\|$	$\|k_{p,7}\|$
D, E, F1	36	44	140°, 7/9 fractional pitch	0.940	0.174	0.776
F2	36	44	180°, full pitch	1	1	1

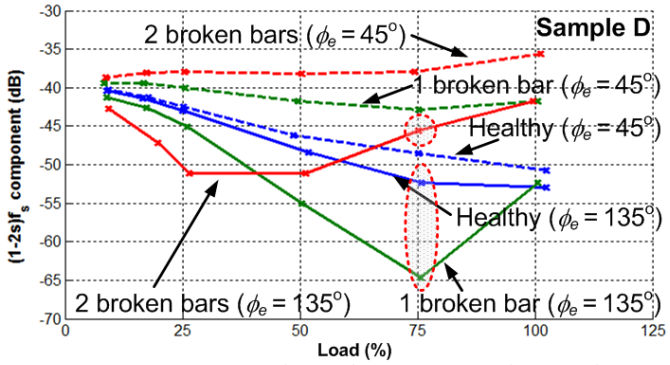

Fig. 8 MCSA measurements of (1-2*s*) f_s components as a function of % rated slip (load) with 0-2 broken bars (sample D) located at ϕ_e = 45° (dotted line) and ϕ_e = 135° (real line)

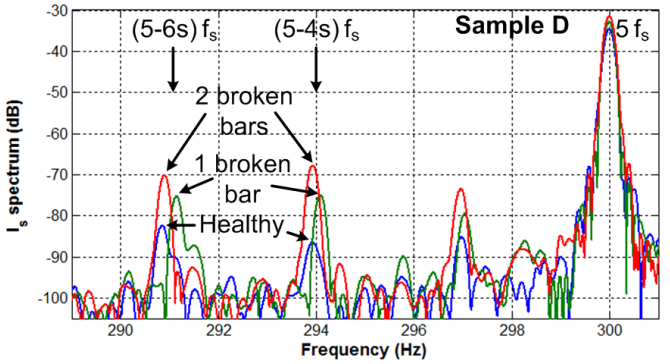

Fig. 9 I_s spectrum showing (5-4*s*) f_s and (5-6*s*) f_s components with 0-2 broken bars (sample D) located at ϕ_e = 135° at 75% rated load

in Fig. 4, and shows that $I_{s,brb,1}$ is not a reliable indicator since it can change depending on the fault location, load, and the amplitude of individual $I_{m,brb,1}$ and $I_{r,brb,1}$ components.

The (5-4s)f_s and (5-6$_s$)f_s components in the I_s spectrum are shown in Fig. 9 for sample D for the case where 0, 1, 2 bars are broken at ϕ_e=135^o under 75% rated load. This corresponds to the 75% rated load condition with 0 to 2 broken bars highlighted in Fig.8, where MCSA based on $I_{s,brb,1}$ fails. Under this condition, the rotor is likely to be misdiagnosed as "faulty" (-52.3 dB) when the rotor is healthy, and as "healthy" (-64.6 dB) when the rotor has 1 broken bar. It can be seen in Fig. 9 that the (5-4s) f_s and (5-6s) f_s components increase with the number of broken bars unlike the (1-2s) f_s component.

The $f_{brb,h}$ components induced by the 5th and 7th space harmonics, (5-4s)f_s, (7-6s)f_s, (5-6$_s$)f_s, and (7-8s)f_s, were observed under different load and fault conditions, and all the components showed a similar trend in that they increase with fault severity. It was concluded after careful observation that the (5-4s)f_s component provides the most consistent and reliable indication of rotor faults. The average of the (5-4s)f_s components obtained 3 times under 25~100% rated load with 0~2 broken bars located at ϕ_e=45^o and 135^o for sample D are shown in Fig. 10. It can be clearly seen that the fault indicator (5-4s) f_s increases with the number of broken bars independent of fault location and load. This shows that the proposed method provides reliable detection of rotor faults, and is immune to the axial duct influence.

The results shown in Figs. 8-10 for sample D are repeated for sample E in Figs. 11-13. The trend in how the N_d=N_p axial ducts influences $I_{s,brb,1}$, and how the $f_{brb,h}$ components change with fault severity is similar to that of sample D. It can be observed in Fig. 11 that the influence of axial ducts is smaller for the case of sample E (smaller $I_{m,brb,1}$). This is due to the narrower flux path behind the axial duct, which shows that the degree of the axial duct interference depends on the rotor axial duct design. For the case where motor is operating at 25% rated load with the rotor fault located at ϕ_e=135^o (highlighted in Fig. 11), the (1-2s)f_s component is relatively high at -53.1 dB for a healthy rotor, and low at -81.0 dB for a rotor with 1 broken bar. It is shown in Fig 12 that the (5-4s)f_s and (5-6s)f_s components increase with fault severity providing reliable detection of rotor faults where MCSA based on (1-2s)f_s produces false indications. The (5-4s)f_s and (5-6s)f_s components under 25~100% rated load with 0~2 broken bars located at ϕ_e=45^o and 135^o are shown in Figs. 13 and 14, respectively, for sample E. The (5-4s)f_s and (5-6s)f_s components shows a clear increase with fault severity independent of fault location and load level, as in the case of sample D.

The (1-2s)f_s and (5-4s)f_s components measured from samples F1 and F2 with 7/9 fractional pitch and full pitch stator winding with 3 broken rotor bars are shown in Fig. 15 to demonstrate one of the limitations of the proposed method. The rotor of sample F is the same as the *Al* die cast rotor of sample D, but without any axial ducts. It can be observed that the increase in the (1-2s)f_s and (5-4s)f_s components is larger for the full pitch winding since fundamental and 5th space harmonic components are relatively larger, as can be seen in Table III. The (1-2s)f_s

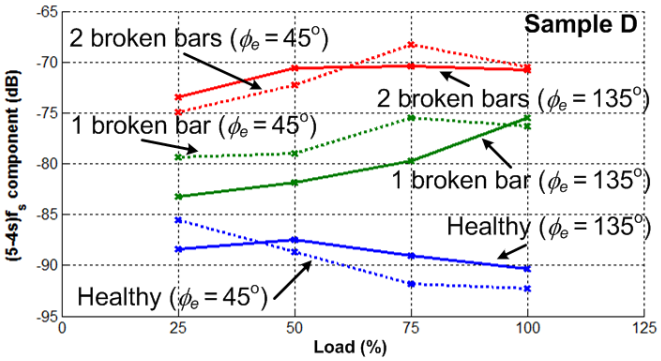

Fig. 10 MCSA measurements of (5-4s) f_s components as a function of % rated slip (load) with 0-2 broken bars (sample D) located at ϕ_e = 45° (dotted line) and ϕ_e = 135° (real line)

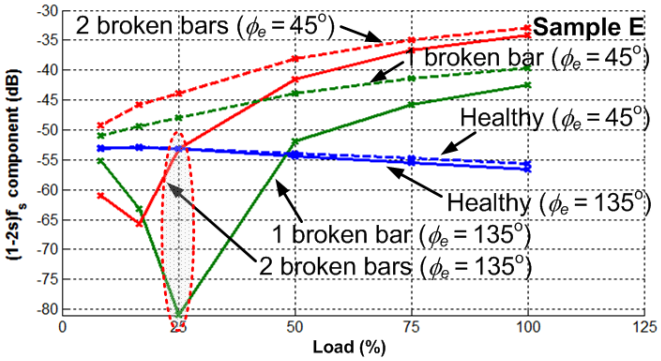

Fig. 11 MCSA measurements of (1-2s) f_s components as a function of % rated slip (load) with 0-2 broken bars (sample E) located at ϕ_e = 45° (dotted line) and ϕ_e = 135° (real line)

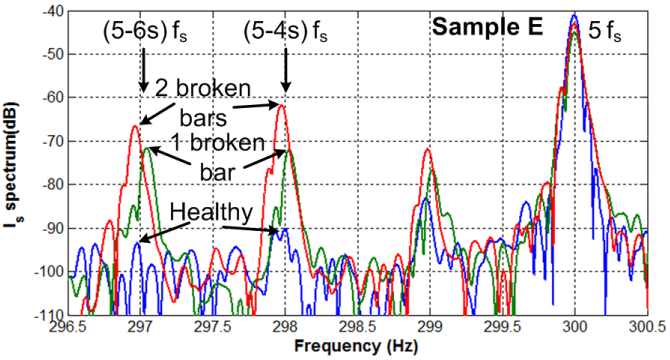

Fig. 12 I_s spectrum showing (5-4s) f_s and (5-6s) f_s components with 0-2 broken bars (sample E) located at ϕ_e = 135° at 25% rated load

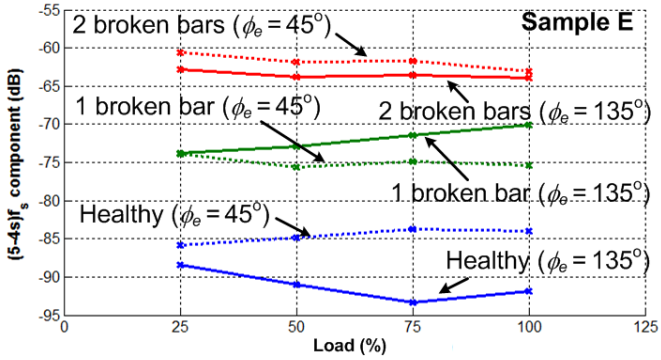

Fig. 13 MCSA measurements of (5-4s) f_s components as a function of % rated slip (load) with 0-2 broken bars (sample E) located at ϕ_e = 45° (dotted line) and ϕ_e = 135° (real line)

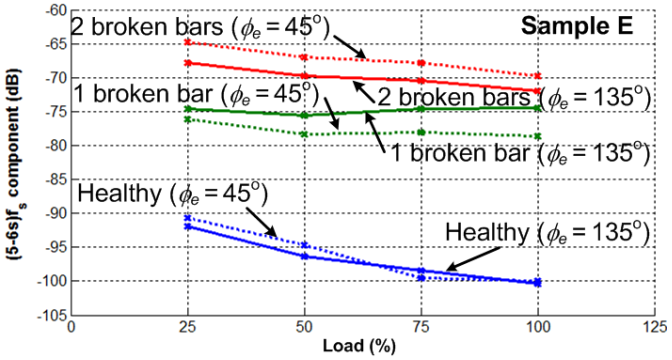

Fig. 14 MCSA measurements of (5-6s) f_s components as a function of % rated slip (load) with 0-2 broken bars (sample E) located at $\phi_e = 45^o$ (dotted line) and $\phi_e = 135^o$ (real line)

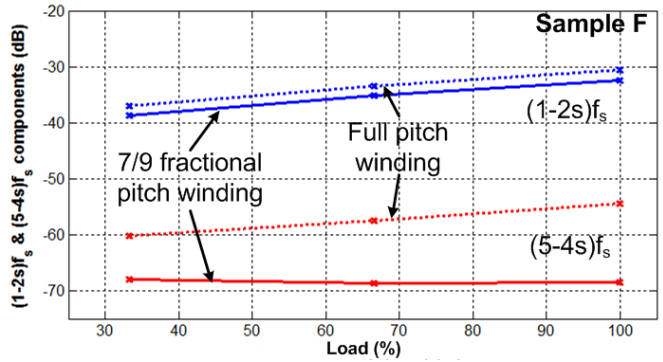

Fig. 15 MCSA measurements of (1-2s)f_s and (5-4s)f_s components for fractional pitch (sample F1) and full pitch (sample F2) winding with 3 broken rotor bars

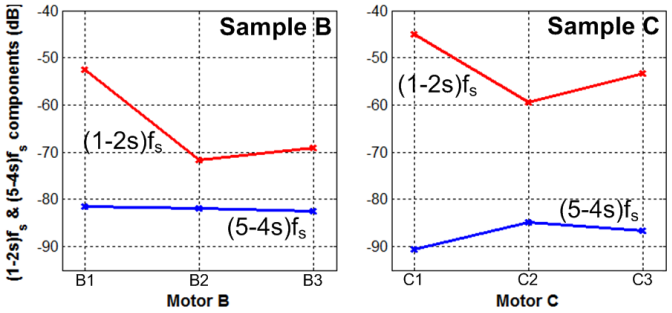

(a) (b)

Fig. 16 MCSA measurements of (1-2s)f_s and (5-4s)f_s components for motors with false rotor fault alarms (a) motor samples B1, B2, B3 and (b) motor samples C1, C2, and C3

and (5-4s)f_s components are typically below -60 dB and -80 dB, respectively, when measured for healthy motors, as can be seen in Figs. 10, and 13. The difference in the increase is substantial for the (5-4s)f_s component, where the pitch factor is higher for the full pitch winding by 10-15 dB. The results of Fig. 15 shows that the increase in the fault indicator depends on the stator winding structure, and this is one of the potential limitations of determining fault severity based the $f_{brb,h}$ components. The results shown in Figs. 10, 13, and 15 also show that the amplitude of the $f_{brb,h}$ components are insensitive to load compared to the $f_{brb,1}$ components, which is an advantage.

The (5-4s)f_s and (1-2s)f_s components of the 6.6 kV, 350 kW and 280 kW motor samples B and C of Fig. 2 with false rotor fault alarms are shown in Fig. 16. The (5-4s) f_s components for identical motors B1, B2, and B3 were measured at -81.5, -81.8, and -82.6 dB, respectively. This is very consistent compared to the (1-2s) f_s components that have a variation of 20 dB, as shown in Figs. 3(b) and 16(a). A similar trend can be observed for motors C1, C2, and C3, where the (5-4s) f_s components are very low and consistent at -90.5, -84.8, -86.6 dB compared to the (1-2s) f_s components that have a variation of 15 dB. In fact, the (5-4s) f_s component of motor C1 with the highest (1-2s) f_s component is the lowest, as can be seen in Figs. 3(c) and 16(b). The results of Fig. 16 show that inspection of the rotor due to the false indications produced by the (1-2s) f_s component could have been avoided if the (5-4s) f_s component had been monitored. If the proposed method had been applied for screening out the false alarm, the plant that disassembled sample C could have saved 20,000 USD on motor inspection. The test results on the 6.6 kV motor (samples B and C) and the lab samples (samples D, E, and F) clearly show that false rotor fault alarms can be avoided by analyzing the $f_{brb,h}$ component with MCSA.

V. Conclusion

On-line monitoring of space harmonics induced rotor fault components, $f_{brb,h}$, with MCSA is proposed as a reliable means of detecting rotor faults independent of axial ducts. Motor outage and inspection due to false indications produced by axial ducts is currently a common problem in the field with no solution other than off-line or startup testing. An analysis shows that space harmonic flux cannot penetrate into the rotor to produce false alarms due to the high slip between the rotor and space harmonic wave, making the $f_{brb,h}$ components a reliable fault indicator. The effectiveness of the proposed method was verified on custom built rotors and also on 6.6kV motors in the field that were misdiagnosed with rotor faults. The experimental results clearly show that the proposed fault indicator is immune to the axial duct influence, and can be used for detecting the fault and screening out false alarms. The trend of the 1) increase in the $f_{brb,h}$ components with time and 2) comparison of the $f_{brb,h}$ components measured on motors of identical design can be used as an effective measure of false alarms.

The space harmonics ($f_{brb,h}$)-based MCSA method, which has been applied to this problem for the first time in this work, is expected to help prevent unnecessary inspection and/or loss of production due to false broken bar indications that frequently occur in the field. It also provides reliable diagnosis of motors with axial duct induced magnetic asymmetry, which was only possible with off-line or startup test methods. The proposed algorithm is currently being successfully applied in the field for screening out false positive indications when the (1-2s)f_s broken bar frequency component of on-line MCSA exceeds the alarm level.

Acknowledgement

This research was partially supported by the Basic Science Research Program through the National Research Foundation

of Korea (NRF) funded by the Ministry of Education, Science and Technology (NRF-2013R1A1A2010370), and partially by the Human Resources Development program(20134030200340) of the Korea Institute of Energy Technology Evaluation and Planning (KETEP) grant funded by the Korea government Ministry of Trade, Industry and Energy.

REFERENCES

[1] C. Concari, G. Franceschini, C. Tassoni, A. Toscani, "Validation of a faulted rotor induction machine model with an insightful geometrical interpretation of physical quantities," *IEEE Trans. on Ind. Electron.*, vol. 60, no. 9, pp. 4074-4083, Sept. 2013..

[2] Y. Kim, Y. Youn, D. Hwang, J. Sun, and D. Kang, "High-resolution parameter estimation method to identify broken rotor bar faults in induction motors," *IEEE Trans. on Ind. Electron.*, vol. 60, no. 9, pp. 4103-4117, Sept. 2013.

[3] A. Soualhi, G. Clerc, and H. Razik, "Detection and diagnosis of faults in induction motor using an improved artificial ant clustering technique," *IEEE Trans. on Ind. Electron.*, vol. 60, no. 9, pp. 4053-4062, Sept. 2013.

[4] G.B. Kliman, R.A. Koegl, J. Stein, R.D. Endicott, and M.W. Madden, "Noninvasive detection of broken rotor bars in operating induction motors," *IEEE Trans. on Ener. Conv.*, vol. 3, no. 4, pp.873-879, Dec 1988.

[5] W. Thomson, "Recent (2005-2006) case histories on the application of motor current signature analysis to detect broken rotor bars," *Proc. of Iris Rotating Machine Conference (IRMC)*, 2006.

[6] I.M. Culbert, and W. Rhodes, "Using current signature analysis technology to reliably detect cage winding defects in squirrel-cage induction motors," *IEEE Trans. on Ind. Appl.*, vol.43, no.2, pp.422-428, Mar./Apr. 2007.

[7] W.T. Thomson, "On-line current monitoring – the influence of mechanical loads or a unique rotor design on the diagnosis of broken rotor bars in induction motors," *Proc. of ICEM*, pp. 1236-1240, 1992.

[8] A. Bellini, et al., "On-field experience with on-line diagnosis of large induction motors cage failures using MCSA," *IEEE Trans. on Ind. Appl.*, pp. 1045-1053, vol. 38, no. 4, July/Aug. 2002.

[9] S. Lee, J. Hong, S.B. Lee, E. Wiedenbrug, M. Teska, and H. Kim, "Evaluation of the influence of rotor axial air duct design on condition monitoring of induction motors," *IEEE Trans. on Ind. Appl.*, vol. 49, no. 5, pp. 2024-2033, Sept./Oct. 2013.

[10] C. Yang et. al., "Reliable detection of induction motor rotor faults under the rotor axial air duct influence," *Proc. of IEEE ECCE*, pp. 2508-2515, Raleigh, NC, Sept. 2013.

[11] B.D. Evans, "Induction motor case histories: a focus on electrically related phenomena," *Proc. of Vibration Institute Annual Meeting*, 2009.

[12] *Testing of squirrel cage rotors*, Electrical Apparatus Service Association Inc., EASA Tech. Note 23, 2003.

[13] T.A. Lipo, *Introduction to AC machine design*. Madison, WI: Wisconsin Power Electronics Research Center, Univ. Wisconsin, 2004.

[14] T.J. Sobczyk, and W. Maciolek, "Diagnostics of rotor-cage faults supported by effects due to higher MMF harmonics," *Proc. of Power Tech Conf.*, vol. 2, pp. 5-9, June 2003.

[15] M. Riera-Guasp, J. Pons-Llinares, F. Vedreno-Santos, J.A. Antonino-Daviu, M. Fernandez Cabanas, "Evaluation of the amplitudes of high-order fault related components in double bar faults," *Proc. of IEEE Int'l Sym. on Diagn. for Elec. Mach., Pwr. Electr. and Drives*, pp. 307-315, Sept. 2011.

[16] H. Henao, H. Razik, and G.A. Capolino, "Analytical approach of the stator current frequency harmonics computation for detection of induction machine rotor faults," *IEEE Trans. on Ind. Appl.*, vol. 41, no. 3, pp. 801-807, May/June 2005.

[17] B. Akin, U. Orguner, H.A. Toliyat, and M. Rayner, "Low order PWM inverter harmonics contributions to the inverter-fed induction machine fault diagnosis," *IEEE Trans. on Ind. Electron.*, vol.55, no.2, pp. 610-619, Feb. 2008.

[18] C.H. De Angelo, G.R. Bossio, J.M. Bossio, G.O. Garcia, "Broken bar detection in single-phase reciprocating compressors," *Proc. of IEEE Ind. Electron. Conf.*, pp. 1125-1130, 2008.

[19] C. Bruzzese, "Analysis and application of particular current signatures (symptoms) for cage monitoring in nonsinusoidally fed motors with high rejection to drive load, inertia, and frequency variations," *IEEE Trans. on Ind. Electron.*, vol. 55, pp. 4137-4155, Dec. 2008.

[20] G.M. Joksimovic, J. Riger, T.M. Wolbank, N. Peric, M. Vasak, "Stator-current spectrum signature of healthy cage rotor induction machines," *IEEE Trans. on Ind. Electron.*, vol. 60, no. 9, pp. 4025-4033, Sept. 2013.

[21] S.H. Kia, H. Henao, G.-A. Capolino, "Some digital signal processing techniques for induction machines diagnosis," *Proc. of IEEE SDEMPED*, pp. 322-329, Sept. 2011.

[22] Y. Kim, Y. Youn, D. Hwang, J. Sun, and D. Kang, "High-resolution parameter estimation method to identify broken rotor bar faults in induction motors," *IEEE Trans. on Ind. Electron.*, vol. 60, no. 9, pp. 4103-4117, Sept. 2013.

[23] M.Y. Kaikaa, M. Hadjami, "Effects of the simultaneous presence of static eccentricity and broken rotor bars on the stator current of induction machine," *IEEE Trans. on Ind. Electron.*, vol. 61, no. 5, pp. 2452-2463, May 2014.

Chanseung Yang (S'12) received the B.S. degree in Electrical Engineering in 2012 from Korea University, Seoul, Korea, where he is currently working toward the Ph.D degree. In 2012, he was an Intern with the Universitat Politècnica de València (UPV), Valencia, Spain. In 2014, he was an Intern with the Universtat di Bologna, Bologna, Italy. His research interests are in condition monitoring and analysis of electric machinery.

Taejune Kang (S'11) received his B.S. degree in Electrical Engineering from Korea University, Seoul, Korea, in 2011. He is currently pursuing his Ph.D. degree in electrical engineering at Korea University, Seoul, Korea. He was an Intern with the Universitat Politècnica de València (UPV), Valencia, Spain in 2012, and an Intern with the Universtat di Bologna, Bologna, Italy in 2014. His research interests are in stator winding insulation testing and condition monitoring and diagnostics of electric machinery

Sang Bin Lee (S'95-M'01-SM' 07) received the B.S. and M.S. degrees from Korea University, Seoul, Korea in 1995 and 1997, respectively, and his Ph.D. degree from Georgia Institute of Technology, Atlanta, GA in 2001, all in Electrical Engineering.

From 2001 to 2004, he was with General Electric Global Research Center (GRC), Schenectady, NY. At GE GRC, he developed an inter-laminar core fault detector for generator stator cores, and worked on insulation quality assessment for electric machines. From 2010 to 2011, he was with the Austrian Institute of Technology, Vienna, Austria, as a Research Scientist where he worked on condition monitoring of PM synchronous machines. Since 2004, he has been a professor of Electrical Engineering at Korea University, Seoul, Korea. His current research interests are in protection, monitoring and diagnostics, and analysis of electric machines and drives.

Dr. Lee was the recipient of the nine prize paper awards from the IEEE Power Engineering Society, the Electric Machines Committee of the IEEE Industry Applications Society, and the Technical Committee on Diagnostics of the IEEE Power Electronics Society. He serves as a Distinguished Lecturer (2014-2015) for IEEE IAS, and an Associate Editor for the IEEE Transactions on Industry Applications for the IEEE IAS Electric Machines Committee.

Ji-Yoon Yoo received the B.S. and M.S. degrees in from Korea University, Seoul, Korea, in 1977 and 1983, respectively, and the Ph.D. degree in from Waseda University, Tokyo, Japan, in 1987, all in electrical engineering.

From 1987 to 1991, he was an Assistant Professor in the Department of Electrical Engineering, Changwon National University. Since 1991, he has been with the Department of Electrical Engineering, Korea University, where he is currently involved in the research on control of electric machines and drives and power electronics converters. His research interests include modeling, analysis, and control of hybrid electric vehicle systems, and flexible ac transmission systems.

Alberto Bellini (S'96, M'99) was born in Italy in 1969. He received the Laurea (M.S.) degree in electronic engineering and the Ph.D. degree in computer science and electronics engineering from the University of Bologna, Bologna, Italy, in 1994 and 1998, respectively. From 1999 to 2004, he was with the University of Parma, Parma, Italy. He was an Honorary Scholar with the University of Wisconsin, Madison, during 2000. Since 2004, he has been with the University of Modena and Reggio Emilia, Reggio Emilia, Italy, where he is currently an Assistant Professor of electric machines and drives. He is the author or coauthor of more than 80 papers, one textbook, and is the holder of three industrial patents. His research interests include electric drive design and diagnosis, power electronics, and signal processing for industrial applications and audio. Dr. Bellini serves as an Associate Editor of the IEEE TRANSACTIONS ON INDUSTRIAL ELECTRONICS. He was the recipient of the First Prize Paper Award from the Electric Machines Committee of the IEEE Industry Applications Society in 2001.

Luca Zarri (M'05, SM'12) was born in Bologna, Italy, in 1972. He received the M. Sc. in Electrical Engineering, with honors, and the Ph.D. degree from the University of Bologna, Bologna, Italy, in 1998 and 2007, respectively. He worked as a freelance software programmer from 1989 to 1992 and as a plant designer with an engineering company from 1998 to 2002. In 2003 he became a Laboratory Engineer with the Department of Electrical Engineering, University of Bologna. Since 2005 he has been an Assistant Professor with the same department. He is author or co-author of more than 100 scientific papers. His research activity concerns the control of power converters and electric drives. He is a member of the IEEE Industry Applications, IEEE Power Electronics and IEEE Industrial Electronics Societies. He serves as Associate Editor for IEEE Transactions on Industry Applications for the IEEE IAS Electric Machines Committee, and has served as Guest Associate Editor for some special issues on IEEE Transactions on Industry Applications and IEEE Journal of Emerging and Selected Topics in Power Electronics.

Fiorenzo Filippetti (M'00) received the M.S. degree in electrical engineering from the University of Bologna, Bologna, Italy, in 1970. In 1976, he became an Assistant Professor in the Department of Electrical, Electronics and Information Engineering G. Marconi (DEI), University of Bologna, where he is currently a Full Professor of electrical machines. He was a visiting professor at the University Claude Bernard, Centre de Gnie Electrique de Lyon (CEGELY), University Claude Bernard, Lyon, France, and the University of Picardie Jules Verne, Amiens, France. His main research interests include simulation and modeling of electric circuits and systems, and the study and application of condition-monitoring and fault-detection techniques for ac electrical machines. He was the recipient of the IEEE PELS Diagnostic Achievement Award in 2013, and 3 Prize Paper Awards at IEEE IAS and SDEMPED conferences.